33RD CONGRESS
OF THE INTERNATIONAL COUNCIL
OF THE AERONAUTICAL SCIENCES
STOCKHOLM, SWEDEN, 4-9 SEPTEMBER, 2022

ICAS 2022 SWEDEN

EXPERIMENTAL STUDY ON NON-COMMAND MOTION CHARACTERISTICS OF SMALL ASPECT RATIO FLYING WING

Shen Yanjie[1,2], Feng Shuai[1,2], Wang Yanling[1,2], Bu Chen[1,2], Tan Hao[1,2], Mu Weiqiang[1,2], Chen Hao[1,2]

[1]AVIC Aerodynamics Research Institute, Harbin 150001, China;

[2]Aviation Key Laboratory of Science and Technology on Low Speed and High Reynolds Number Aerodynamic Research, Harbin 150001, China

Abstract

The small aspect ratio flying wing layout has become an advanced fighter development platform due to its high stealth and high aerodynamic efficiency. The particularity of the layout reduces the lateral stability, which makes it face the problem of wing rock instability and affects the maneuvering of the aircraft. performance and flight quality. Through wind tunnel test and numerical simulation method, the rock characteristics and mechanism of small aspect ratio flying wing scalar wing were comprehensively analyzed, and a nonlinear aerodynamic model coupled with the effect of roll angular rate was developed. The results show that the small aspect ratio flying wing layout has the wing rock problem after the pitch angle of 28° , and the curve of the roll moment coefficient with the roll angle in the limit cycle oscillation process is not a stable hysteresis loop . During the oscillation process of the limit cycle, the roll damping derivative changes with the roll angle rate as a quadratic function, which makes the roll moment coefficient hysteresis loop in a clockwise state. The influence of the roll angle rate is introduced into the conventional dynamic derivative model, and the simulation limit can be accurately predicted. Ring oscillation.

Keywords: small aspect ratio flying wing layout; wing rock; limit cycle oscillation; aerodynamic model; wind tunnel test.

1. Introduction

The small aspect ratio flying wing layout has excellent performances such as high stealth, high aerodynamic efficiency, low wing load, and low structural weight.

With the increase of the angle of attack, the small aspect ratio of the flying wing and the large swept leading edge will induce complex vortex flow. When the maneuvering flight with a high angle of attack is performed, asymmetric split flow and vortex rupture will appear. These complex flows will Unpredictable aerodynamic forces and moments are induced on the body, so that the aircraft will make corresponding flight movements. Because this kind of flight motion is not the command result obtained by manipulating a certain aerodynamic control surface according to the command of the pilot, but the flight motion that is not controlled by the pilot due to the complex flow induced by the aircraft running at a large angle of attack. It is called uncommented flight motion [1]. Obviously, the appearance of such non-command movements not only affects the high maneuverability of fighters and the implementation of air combat targets, but also poses a serious threat to the safe flight of fighters.

Since the 1980s, a lot of research has been done on this, and scholars have used wind tunnel tests and numerical simulations to solve the problem of F-4, F-5, F-14, X-29A and the wing rock problem with vertical tail flying wing layout. The results show that the generation of the wing

rock problem is related to the flow separation of the wing surface induced by the drop tank, the leading-edge slat, the leading-edge strip and the nose tip, and the lack of roll damping is the main cause of the limit cycle oscillation [2]. In 2003, the Abrupt Wing Stall (AWS) project developed the Free to ROLL (FTR) method, determined the wing rock problem criterion, established a comprehensive analysis method based on wind tunnel test, CFD and modeling simulation, and passed the F/A -18E, F/A-18C, AV-8B and F-16C four layouts of the test [3-7] and analysis [8-16], verified the reliability of the comprehensive analysis method, established a comprehensive analysis of the wing rock problem system. Owens et al. evaluated the wing rock quality factor under various wing configurations of the F-35, and studied and verified the control effect of the leading-edge slat clearance on the wing rock movement [17]. Chung et al. studied the rock characteristics and mechanism of the T-50 trainer wing, and the roll moment coefficient changes with the roll angle in a figure-eight shape [18]. Ma Baofeng et al. conducted an experimental study on the rock-and-roll characteristics of the wing-body combination under a high angle of attack, focusing on the analysis of the effects of tip disturbance, wing position, and Reynolds number on the rock-and-roll motion of the wing [19-22]. Nguyen et al. used energy exchange technology to analyze the physical mechanism of driving limit cycle oscillation, and considered that the curve of roll torque versus roll angle when limit cycle oscillation occurred showed a double 8-figure structure, which was verified by wind tunnel test of large swept delta wing layout [23].

In this paper, the wind tunnel test results of free rolling motion of small aspect ratio flying wings are analyzed, and the variation law of rolling moment coefficient during limit cycle oscillation is studied. The nonlinear effect of the roll angle rate on the dynamic derivative was introduced into the mathematical model of the roll moment, and the prediction of the stable clockwise sluggish-induced wing rock motion was realized.

2. FTR dynamic wind tunnel test

2.1 Test equipment and model

The Flying-wing Dynamic Model (FDM) studied in this paper is a low-aspect-ratio planform model with a leading-edge sweep angle of 65-degree. As shown in Figure 1, the root chord is 1.3927m, the wingspan is 1.0391m, the reference chord is 0.8691m, and the reference area, is 0.6992m2. The moment reference center is coincided with the rotation center which is 0.7432m behind the head point.

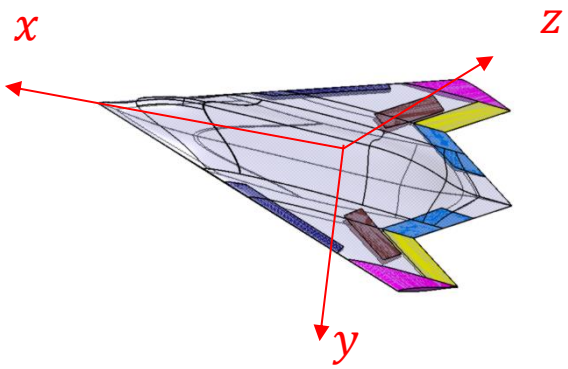

Figure 1 – The planform of FDM configuration.

The test was carried out in the FL-51 wind tunnel of the AVIC Aerodynamics Research Institute, as shown in Figure 2. The FL-51 wind tunnel is a low-speed backflow wind tunnel featuring dynamic tests. It has interchangeable open/closed double test sections. 100m/s (close test section) and 85m/s (open test section), in which the free to rolling (FTR) test are carried out in

the open test section.

(a) FL-51 wind tunnel closed test section

(b) FL-51 wind tunnel opening test section

Figure 2 – FL-51wind tunnel closed and open test sections.

The FTR test adopts a high-angle-of-attack test support system. The size and shape of the FTR device are the same as those of the test balance. The front and rear ends are connected to the model and support rod through cone fit, as shown in Figures 3 and 4. The front end of the FTR device is a free end, which is connected to other parts through bearings. The rolling damping and inertia of the device are ignored during the test. In the FTR device, the center of mass of the model is located on the axis of the tail support mechanism, and the rolling degree of freedom along the longitudinal axis of the model body is not constrained, so that the model can revolve around the x -axis of the body axis. During the time history measurement, the roll angle time history is recorded by the rotary encoder.

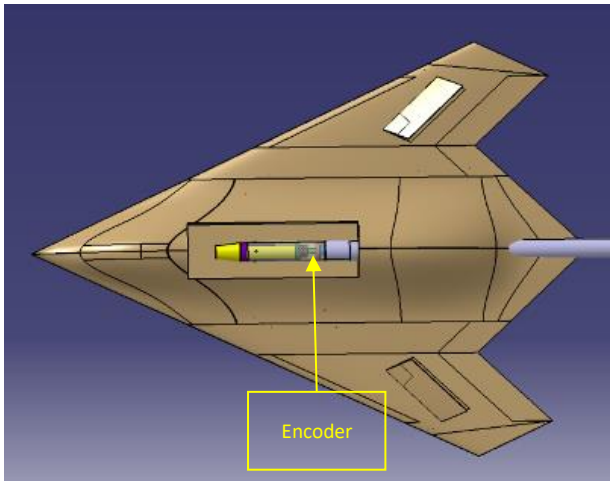

(a) Schematic diagram of mechanism connection

(b) Physical map of the organization

Figure 3 – Free rolling mechanism.

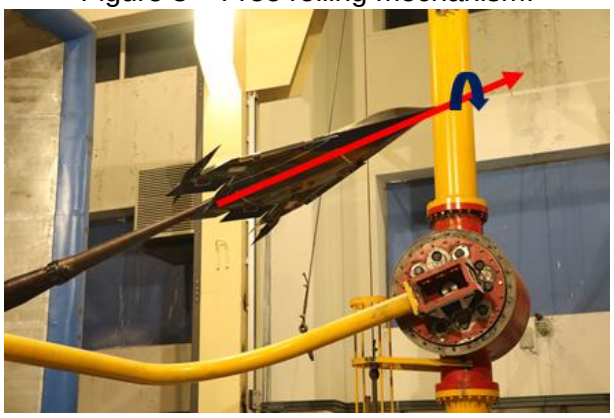

Figure 4 – Free Roll Test Diagram.

2.2 Wing rock characteristics of lower wing at different pitch angles

During the FTR test, the wind speed remained unchanged, the model's roll degree of freedom was always released, and the model's pitch angle increased stepwise from 0°. The pitch angle is first increased from 0° to 90° and then decreased to 0°. The pitch angle sequence is the same in the two processes of ascending and descending. Figure 5 shows the curve of roll balance angle and motion amplitude in the state of all zeros of the rudder surface , in which θ are pitch angle and ϕ roll angle , the model rolls to the right as positive, the fishbone line represents the roll oscillation motion range of the model, and the diamond shape Represents the center position of the model's oscillating motion, and the test wind speed is V = 20 m/s . It can be seen from the figure that after the pitch angle of 28 °, the model exhibits a significant uncommand roll motion.

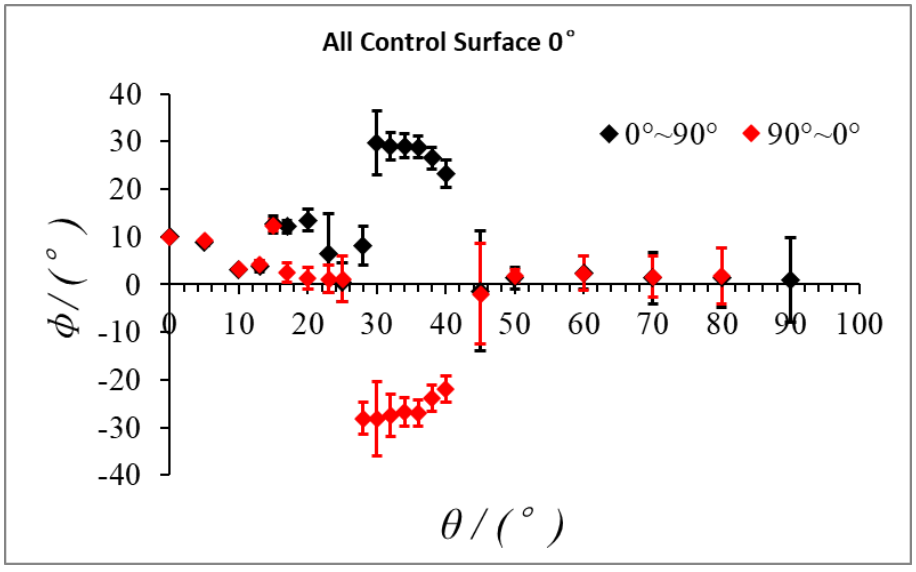

Figure 5 – Rolling balance angle and motion amplitude

Figure 6 shows the $\theta = 30°$ time -wing rock time history, phase plane and spectral characteristic curves. When the pitch angle is 30°, it is a typical limit cycle oscillation state. Although the amplitude changes slightly with time, the frequency is always stable at 1.40 Hz. The phase plane can clearly see the concentric circles of varying diameters, indicating that the oscillation equilibrium position is always maintained at ϕ = 30 ° near.

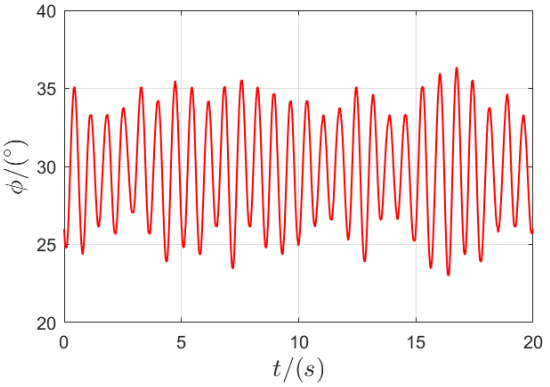

(a) Time history of wing rock ($\theta = 30°$)

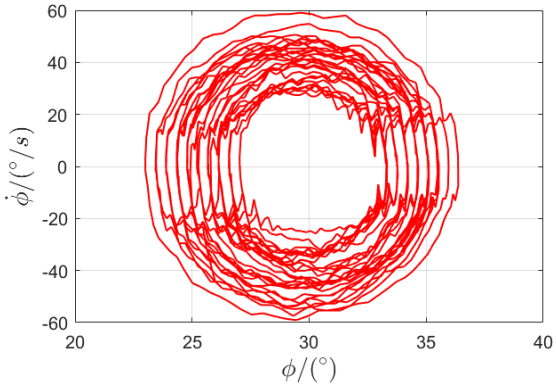

(b) Wing rock phase plane ($\theta = 30°$)

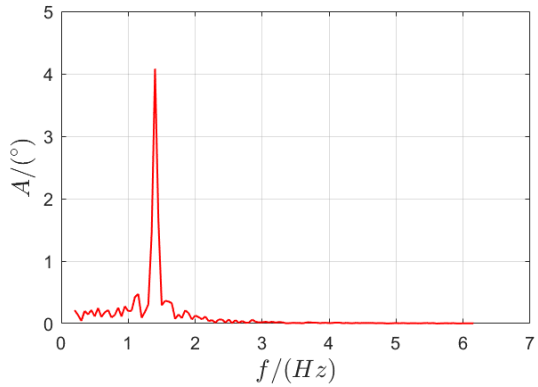

(c) Spectrum characteristic of wing rock ($\theta = 30°$)

Figure 6 – Wing Rock Motion Characteristics.

Figure 7 shows the $C_l \sim \phi$ curves of the limit cycle oscillation process at different starting times. It can be seen that during the oscillation process of the limit cycle at different times, there are different hysteresis loops such as clockwise, counterclockwise and figure 8 in the curve of the roll moment coefficient with the roll angle. This shows that the $C_l \sim \phi$ curve does not necessarily show a stable figure - of -8 or double figure-of-8 in the limit cycle oscillation process of FDM.

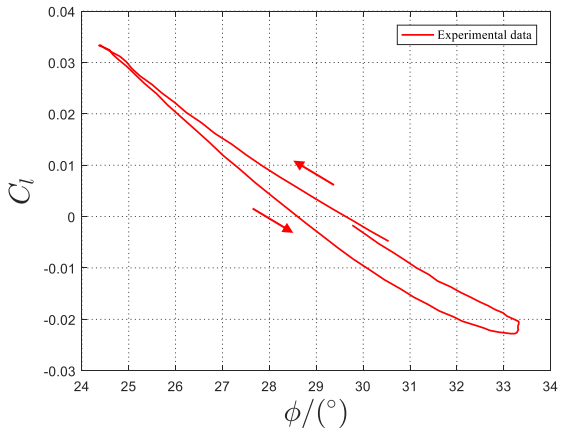

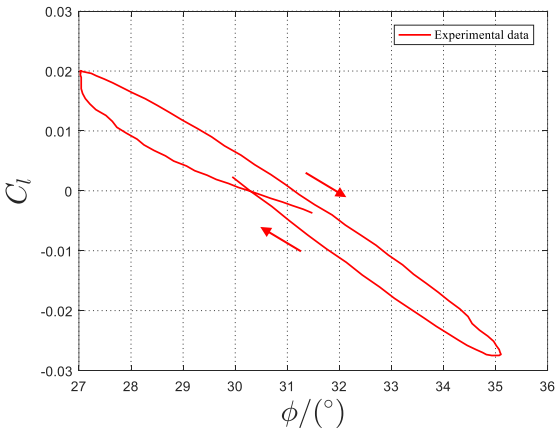

(a) Starting time=0.58s

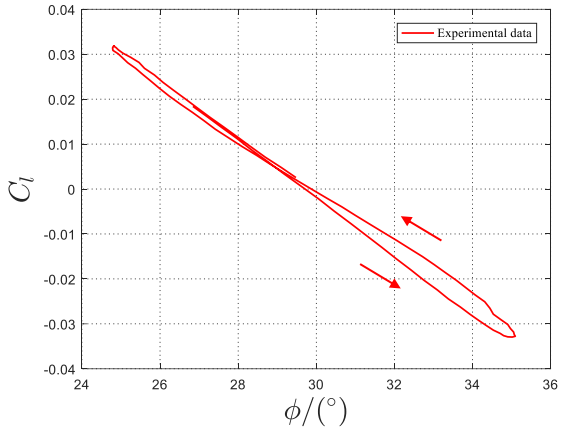

(b) Starting time=2.67s

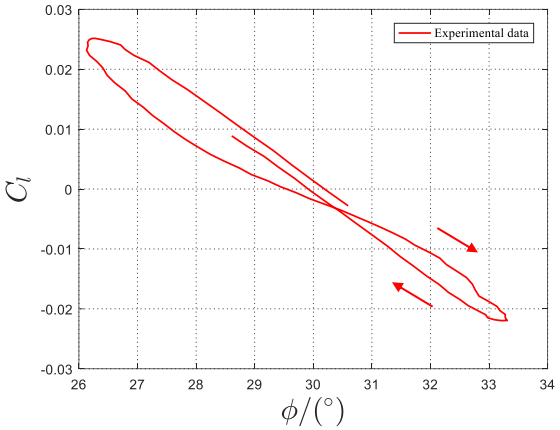

(c) Starting time=4.92s

(d) Starting time=10.5s

Figure 7 – FTR experimental $C_l \sim \phi$ at different time.

3. Wing Rock Numerical Simulation

In order to further analyze the variation characteristics of rolling moment in the limit cycle oscillation process of FDM and establish a limit cycle oscillation prediction model, this paper carried out the numerical calculation of free roll under the state of pitch angle of 30° .

The governing equation for free roll is:

$$\begin{aligned} I_x \dot{p} &= L \\ p &= p_0 + \dot{p} \times dt \\ \phi &= \phi_0 + p \times dt \end{aligned} \tag{1}$$

where: I_x is the x - axis inertia moment, $\dot{p}$ is the roll angular acceleration , p is the roll angular velocity , L is the roll moment, p_0 is the initial angular velocity, ϕ_0 is the initial roll angle, that is, the initial release position, and dt is the time interval.

Release the flying wing model at 30° and 40° , respectively. Use formula (1) to obtain the motion history of its roll angle and roll angular velocity, so as to obtain the motion history curves of different release positions.

Figure 8 shows the comparison curve between the free roll calculation results and the free roll test results released at a roll angle of 30°. The results show that the calculated amplitude, frequency and oscillation equilibrium angle are in good agreement with the experiment, reflecting the oscillation characteristics of the limit cycle of the standard mode of FDM. Figure 9 shows the comparison curve between the CFD calculation results and the rolling static test data. The calculated rolling moment coefficients (including dynamic increments) are basically consistent with the slopes of the static test results. Therefore, the numerical simulation results of free rolling motion can be used for aerodynamic analysis and modeling research.

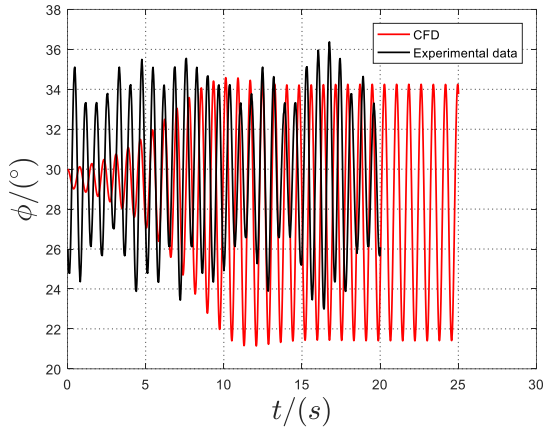

Figure 8 – Comparison of free-to-roll CFD and test results.

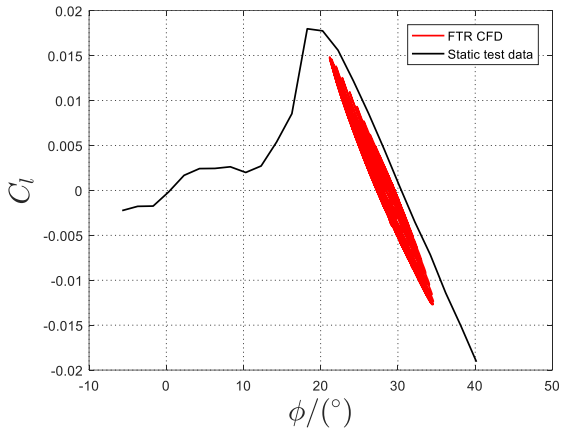

Figure 9 – Free-to-roll CFD and static test result.

Figure 10 shows the curve comparison of the release positions of different roll angles. It can be seen that the initial release position does not affect the rock characteristics of the final wing, that is, the free roll motion characteristics of the standard model are only related to the aerodynamic characteristics of the aircraft body, and have nothing to do with the release position.

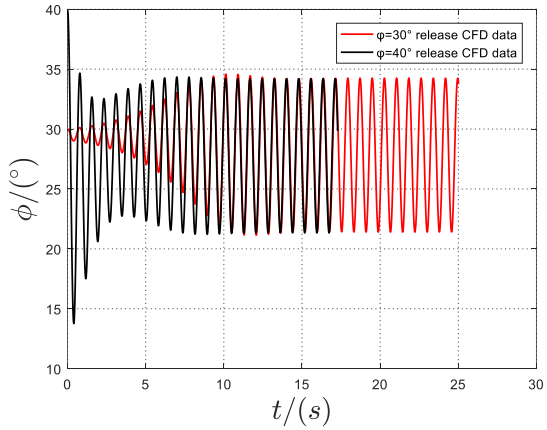

Figure 10 – Free-to-roll CFD results of different roll angle release positions.

Figure 11 shows the variation curve of the roll moment coefficient with the roll angular velocity at different pitch angles. It can be seen that after deducting the roll moment coefficient at zero roll angular velocity , the increment of the roll moment coefficient and the roll angular velocity

have a quadratic function relationship , and the laws are basically the same at each pitch angle.

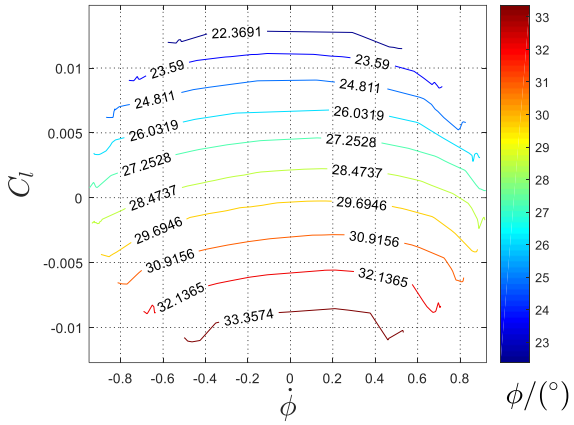

Figure 11 – Curve of rolling moment with rolling angle rate under different pitching angles.

Figure 12 shows the variation curve of roll torque with roll angle under stable limit cycle oscillation. During the limit cycle oscillation process, the roll torque hysteresis loop is generated due to the difference of roll torque increments caused by dynamic motion, in which the arrows indicate the roll torque. Angular velocity direction. From the CFD results, it can be seen that after the FDM enters the stable limit cycle oscillation, the rolling torque hysteresis loop changes in a stable clockwise direction. Literature [2][18][23] believed that the "8" ring or double "8" ring can ensure the energy balance, and then produce the limit cycle oscillation. The reason why the change of rolling torque in the oscillation process of the FDM limit cycle does not conform to the energy balance theory given in the literature [23] is that the basis for the derivation of the capacity balance theory is that the dynamic derivative does not change with the change of the roll angular rate . It can be seen from Figure 11 that the dynamic derivative characteristic of the FDM, does not satisfy this condition, so the FDM limit cycle oscillation has its own unique energy balance process.

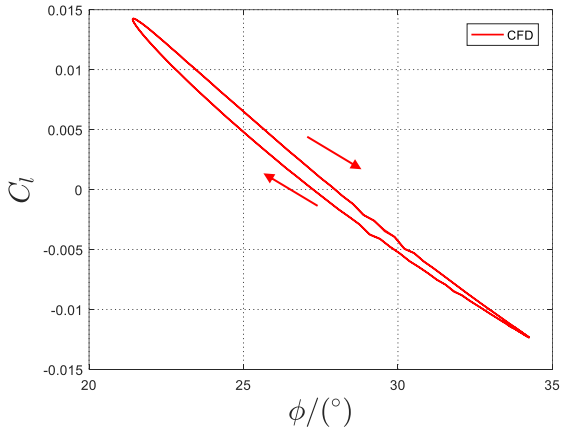

Figure 12 – Hysteresis curve of limit cycle oscillation.

4. Mathematical modeling of wing rock movement

The conventional dynamic derivative model of the rolling moment coefficient can be expressed as:

$$C_l = C_{l_0} + C_{l\phi}(\phi)\phi + C_{l\dot{\phi}}(\phi)\frac{\dot{\phi}b}{2V} \tag{2}$$

where $C_{l\phi}(\phi)$ and $C_{l\dot{\phi}}(\phi)$ denote that the static and dynamic derivatives of the roll moment can be

expressed as a function of the roll angle.

Using the numerical simulation results, the aerodynamic parameters in equation (2) are identified, and the same initial model attitude variables as in the free roll numerical simulation are given. The motion simulation results are shown in Figure 13, where the arrows represent the changing direction of the roll angle, and the black Represents the model simulation results, and red represents the CFD calculation results. Figure 13. (a) (b) (c) It can be seen that the amplitude and frequency of the simulation results of the conventional dynamic derivative model are basically consistent with the CFD calculation results, but there is a significant deviation in the oscillation equilibrium angle of the limit cycle, and the rolling moment coefficient obtained by the simulation is overall Pan down. Figure 13. The hysteresis loop of (d) clearly shows the difference in balance angle and hysteresis loop characteristics. The hysteresis loop in the simulation results of the conventional dynamic derivative model is characterized by double "8" characters, and the hysteresis characteristics are completely different from the CFD calculation results. Although the conventional dynamic derivative model can simulate the spectral characteristics of the limit cycle oscillation, it cannot reflect the variation law of the real rolling moment coefficient.

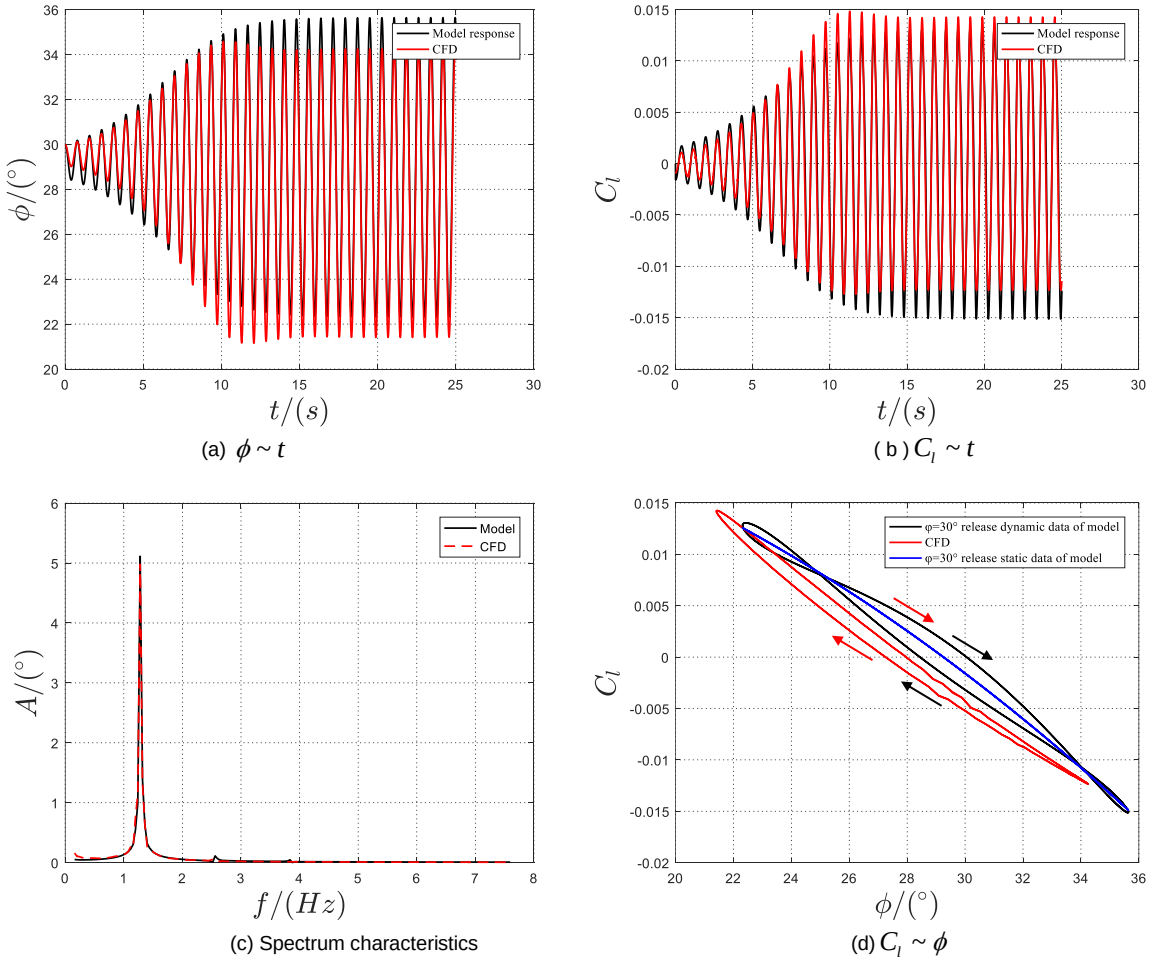

(a) $\phi \sim t$ (b) $C_l \sim t$

(c) Spectrum characteristics (d) $C_l \sim \phi$

Figure 13 – Parameter identification and simulation results of conventional dynamic derivative model.

The main reason for the difference in the limit cycle oscillation is that the conventional dynamic derivative model believes that there is a unique dynamic derivative under a fixed roll angle, which does not change with the change of the roll angular velocity, so the torque increment

caused by the roll angular velocity is a linear curve. However, it can be seen from Fig. 11 that when the pitch angle is 30°, the damping characteristics of the roll moment will change with the change of the roll angle rate, which is inconsistent with the law of the conventional dynamic derivative model. It can be speculated that the discrepancy between the parameter identification results in Fig. 31 and the test results is caused by the inaccurate structure of the conventional dynamic derivative model.

In order to verify the above speculation, the influence of the roll angular velocity on the roll rotational derivative is introduced into the aerodynamic model, and the dynamic derivative model of the coupled roll angular velocity effect is obtained, which is expressed as

$$C_l = c_0 + C_{l\phi}(\phi)\phi + C_{l\dot{\phi}}(\phi,\dot{\phi})\frac{\dot{\phi}b}{2V} \tag{3}$$

where and $C_{l\dot{\phi}}(\phi,\dot{\phi})$ represents the dynamic derivative of the roll moment coefficient as a function of roll angle and roll rate.

The dynamic derivative model coupled with the influence of the roll angle rate is used to identify the parameters of the CFD calculation results, and perform back-test simulation, as shown in Figure 14. After the improvement of the dynamic derivative model, the CFD free roll calculation results released by the roll angle of 30° can be reproduced. The spectral characteristics, limit cycle oscillation equilibrium point, and hysteresis loop characteristics are all consistent with the CFD calculation results.

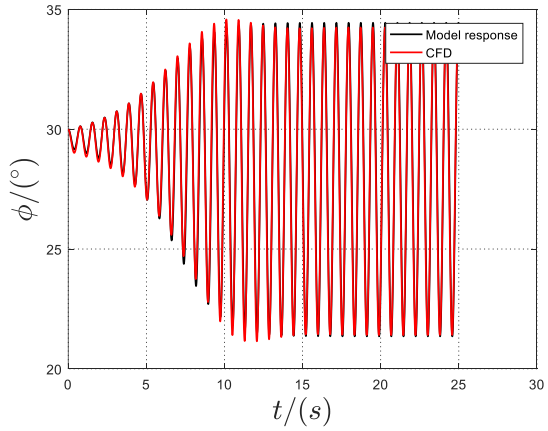

(a) $\phi \sim t$

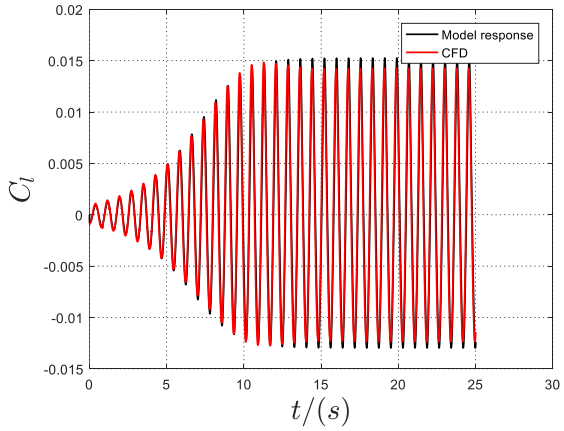

(b) $C_l \sim t$

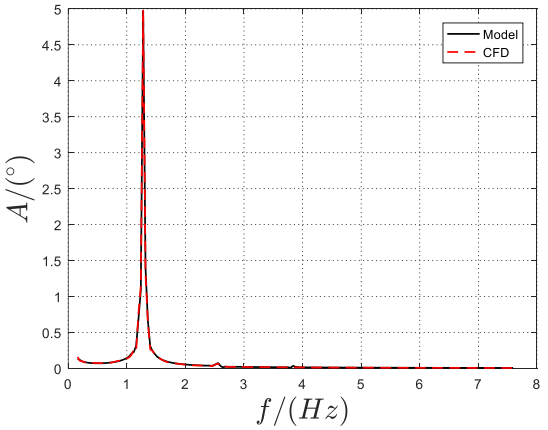

(c) Spectrum characteristics

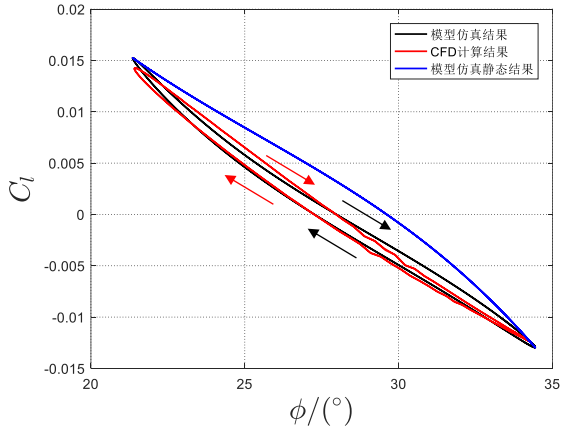

(d) $C_l \sim \phi$

Figure 14 – Parameter identification and simulation results of dynamic derivative model coupling roll rate.

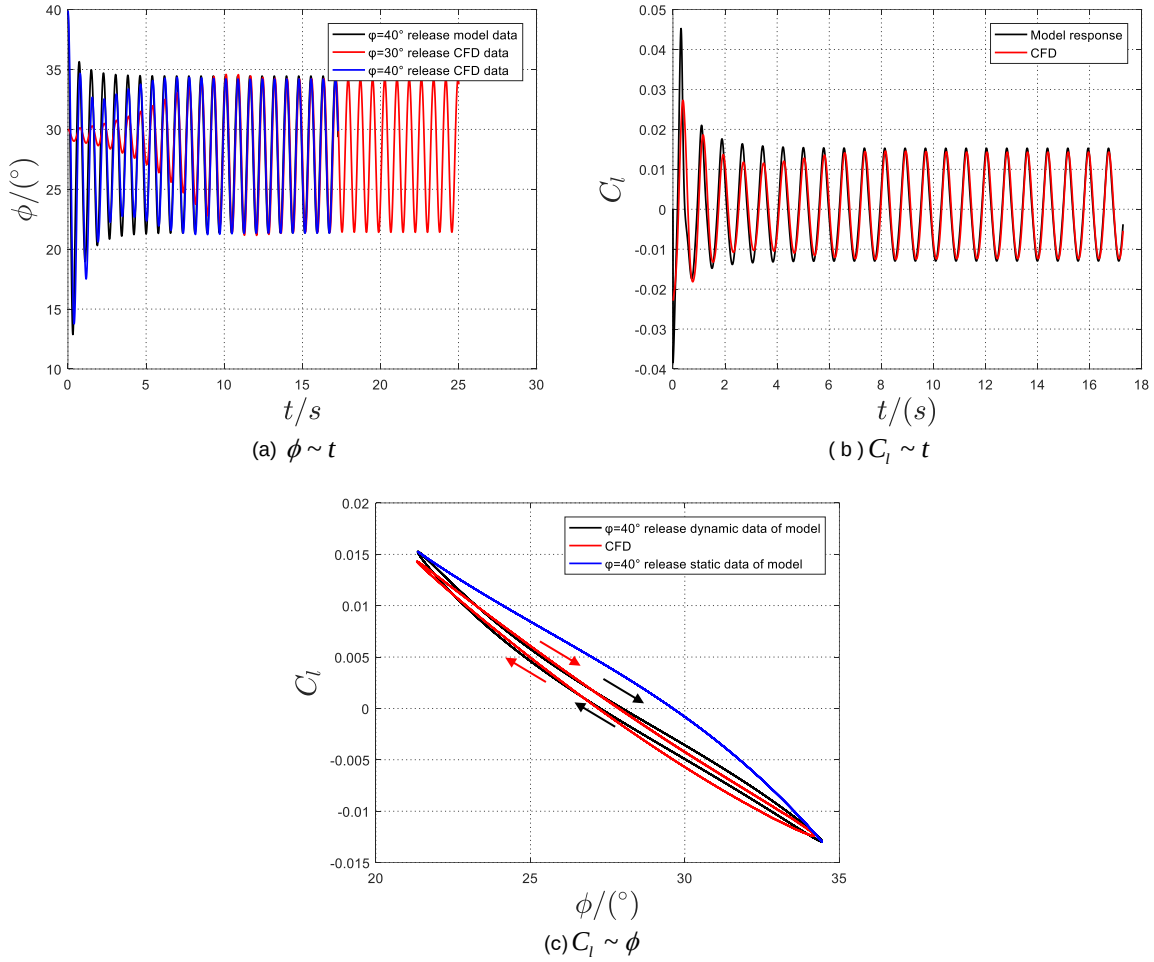

Figure 15 – Simulation results of $\phi = 40^\circ$ release.

Figure 15 compares the $\phi = 40^\circ$ release new model simulation and numerical simulation results. The results show that the prediction results of the improved aerodynamic model are consistent with the numerical simulation results, and it accurately reflects that the different release positions will not change the oscillation characteristics of the limit cycle, but the aerodynamic prediction results around the roll angle of 40° are different from the actual results. This is mainly due to the fact that the data is within the roll angle of 20°~35° when using the 30° roll angle data for parameter identification, and the model motion is within the roll angle range of 15°~40° when the 40° release is performed , so there is an error in data extrapolation. .

In summary, when the rolling moment is in a stable clockwise hysteresis loop, limit cycle oscillation can also be formed. non-linear changes. The modeling process in this paper ignores the influence of unsteady aerodynamic forces, so the limit cycle oscillation characteristics obtained by modeling and simulation always remain unchanged.

5. Conclusion

The conclusions of this study are summarized as follows:

1) FDM has wing rock problem after pitch angle is greater than 28°, and at the same time has serious roll deviation between pitch angle 28° and 45°;

2) During the oscillation process of the limit cycle at a pitch angle of 30° , the curve of the roll moment coefficient with the roll angle is not stable, showing various hysteresis loops such as clockwise, counterclockwise and figure- 8 ;

3) CFD results show that the rolling moment presents a stable clockwise hysteresis loop during the limit cycle oscillation process, and the roll damping derivative presents a quadratic function with the change of the roll angle rate;

4) The influence law of the roll angular rate on the roll damping derivative is introduced into the conventional dynamic derivative model, and the predicted results are consistent with the CFD results.

References

[1] KATZ J. Wing/vortex interactions and wing rock. Progress in Aerospace Sciences, 1999, 35: 727-750.

[2] ROBERT C N; ALAIN P. The unsteady aerodynamics of slender wings and aircraft undergoing large amplitude maneuvers [J], Progress in Aerospace Sciences, 2003, 39(2003): 185-248.

[3] SCHUSTER D, BYRD J. Transonic Unsteady aerodynamics of the F/A-18E at conditions promoting abrupt wing stall: AIAA-2003-0593 [R], Reston: AIAA, 2003.

[4] LAMAR J, CAPONE F, HALL R. AWS figure of merit (FOM) developed parameters from static transonic model tests: AIAA-2003-0745 [R], Reston: AIAA, 2003.

[5] OWENS B, CAPONE F, HALL R, et al. Free-to-roll analysis of abrupt wing stall on military aircraft at transonic speeds: AIAA-2003-0750 [R], Reston: AIAA, 2003.

[6] CAPONE F, OWENS B, HALL R. Development of a free- to- roll transonic test capability: AIAA-2003-0749 [R], Reston: AIAA, 2003.

[7] CAPONE F, HALL B, OWENS B, et al. Recommended experimental procedures for evaluation of abrupt wing stall characteristics: AIAA-2003-0922 [R], Reston: AIAA, 2003.

[8] WOODSON S, GREEN B, CHUNG J, et al. Understanding abrupt wing stall (AWS) with CFD: AIAA-2003-0592 [R], Reston: AIAA, 2003.

[9] FORSYTHE J, WOODSON S. Unsteady CFD calculations of abrupt wing stall using detached- eddy simulation: AIAA-2003-0594 [R], Reston: AIAA, 2003.

[10] GREEN B, OTT J. F/A-18C to E wing morphing study for the abrupt wing stall program: AIAA-2003-0925 [R], Reston: AIAA, 2003.

[11] PARIKH P, CHUNG J. A computational study of the AWS characteristics for various fighter jets: Part I, F/A-18E & F-16C: AIAA-2003-0746 [R], Reston: AIAA, 2003.

[12] CHUNG J, PARIKH P. A computational study of the abrupt wing stall (AWS) characteristics for various fighter jets: Part II, AV-8B and F/A-18C: AIAA-2003-0747 [R], Reston: AIAA, 2003.

[13] WOODSON S, GREEN B, CHUNG J, et al. Recommendations for CFD procedures for predicting abrupt wing stall (AWS): AIAA- 2003-0923 [R], Reston: AIAA, 2003.

[14] ROESCH M, RANDALL B. Flight test assessment of lateral activity: AIAA-2003- 0748 [R], Reston: AIAA, 2003.

[15] KOKOLIOS A, COOK S. Use of piloted simulation for evaluation of abrupt wing stall characteristics: AIAA-2003-0924 [R], Reston: AIAA, 2003.

[16] COOK S, CHAMBERS J, et al. An integrated approach to assessment of abrupt wing stall for advanced aircraft: AIAA-2003-0926 [R], Reston: AIAA, 2003.

[17] OWENS D B, MCCONNELL J, BRANDON J M, et al. Transonic free-to-roll analysis of the F-35(joint strike fighter) aircraft [J]. Journal of Aircraft, 2006, 43(3), 608-615.

[18] CHUNG H S, CHO D, KIM J, et al. Study on wing rock phenomenon of a fighter aircraft using free-to-roll wind tunnel test and dynamic CFD method[C]// American Institute of Aeronautics and Astronautics AIAA Aviation 2019 Forum, Dallas, AIAA, 2019.

[19] MA B F, DENG X Y. Tip-disturbance effects on asymmetric vortex breakdown around a chined forebody [J]. Journal of Aircraft, 2008, 45(4): 1098–1104.

[20] MA B F, DENG X Y, WANG B. Effects of wing locations on wing rock induced by forebody vortices [J]. Chinese Journal of Aeronautics, 2016, 29(5):1226-1236.

[21] WANG B, DENG X Y, MA B F, et al. Effects of tip perturbation and wing locations on rolling oscillation induced by forebody vortice [J]. Acta Mech Sin, 2010, 26(5): 787–791.

[22] MA B F, WANG B, DENG X Y. Effects of Reynolds numbers on wing rock induced by forebody vortices [J]. AIAA Journal, 2017, 1–12.

[23] Nguyen, L. T., Yip L., Chambers J. R., “Self-Induced Wing Rock of Slender Delta Wings”, AIAA Paper 81-1883, AIAA

AFM Conference, Albuquerque, New Mexico, August 1981.

Copyright Statement